Annals of Nuclear Medicine Vol. 15, No. 2, 141–148, 2001

Usefulness of dual-head coincidence gamma camera with thick NaI crystals for nuclear oncology: Comparison with dedicated PET camera and conventional gamma camera with thin NaI crystals

Tomio INOUE,* Noboru ORIUCHI,* Keiko KOYAMA,* Akihiro ICHIKAWA,* Katsumi TOMIYOSHI,* Noriko SATO,* Kunio MATSUBARA,** Hideki SUZUKI,*** Jun AOKI** and Keigo ENDO*

*Departments of *Nuclear Medicine and **Diagnostic Radiology, Gunma University School of Medicine*
*****Department of Medical Information, Gunma Prefectural College of Health Sciences*

Aim: A comparative study of the images obtained with a dual-head coincidence gamma camera with thick NaI crystals (19 mm), a dedicated PET camera with BGO crystals and a conventional gamma camera with thin NaI crystals (9.5 mm) was conducted to clarify the clinical feasibility of a dual-head coincidence gamma camera with thick NaI crystals. ***Methods:*** FDG images of 27 patients with malignant tumors were obtained by means of a dual-head coincidence gamma camera with thick NaI crystal and a dedicated PET camera with BGO crystals. The images of bone scintigraphy in 10 cancer patients obtained with the dual-head coincidence gamma camera were compared with those taken by a conventional dual-head gamma camera with thin NaI crystals. ***Results:*** Patient-basis sensitivity in 27 patients with neoplasms and lesion-basis sensitivity of the dual-head coincidence gamma camera and the dedicated PET camera were 74.1% and 85.2% (n.s.), 66.7% and 72.2% (n.s.), respectively. The tumor to background FDG uptake ratio derived from the coincidence gamma camera was significantly lower than that derived from the dedicated PET camera (mean ± s.d.; 3.48 ± 3.77 vs. 8.12 ± 8.92, $p < 0.0001$), but the tumor to background FDG uptake ratio obtained with both methods correlated well ($r = 0.84$, $p < 0.001$). Similar whole body bone scans were obtained with the dual-head coincidence gamma camera and the conventional dual-head gamma camera in all 10 patients. ***Conclusion:*** These results suggest that the dual-head coincidence gamma camera with thick NaI crystals has potentially high clinical applicability for community hospitals.

Key words: PET, SPECT, malignant tumor, FDG, coincidence gamma camera

INTRODUCTION

POSITRON EMISSION TOMOGRAPHY (PET) with 2-[fluorine-18]fluoro-2-deoxy-D-glucose (FDG) is recognized as a useful radiologic examination for diagnostic oncology,[1–3] but the clinical use of FDG PET has been limited due to the expense involved in the installation of the dedicated PET scanner and in-house cyclotron, and the complexity of on-site synthesis of FDG. The recent development of a cyclotron-accelerator system equipped with automated synthesis technology and the commercial delivery system for FDG are accelerating the widespread expansion of FDG imaging.[1–3] Utilization of a less expensive gamma camera for positron detection also presented diagnostic challenges to the widespread use of FDG imaging. Initially, a gamma camera equipped with ultra-high energy collimators (511 keV SPECT), specially designed for 511 keV annihilation photon detection, was developed and clinically evaluated,[4,5] but FDG imaging with 511 keV SPECT was of limited value in detecting tumors because of its poor spatial resolution and low detection efficiency.[4,5]

In 1995, a gamma camera with a coincidence electronics circuit (coincidence gamma camera) and NaI crystal,

Received October 12, 2000, revision accepted February 14, 2001.

For reprint contact: Tomio Inoue, M.D., Department of Nuclear Medicine, Gunma University School of Medicine, 3–39–22, Showa-machi, Maebashi, Gunma 371–8511, JAPAN.
E-mail: tomioi@med.gunma-u.ac.jp

a relatively inexpensive device for FDG imaging, was developed by Muehllehner et al.[6] It was also an alternative to a dedicated PET camera using the expensive bismuth germanate (BGO). Nevertheless, a thin NaI crystal employed in the initial coincidence gamma camera had the drawback of low efficiency at stopping high energy gamma rays, such as 511 keV photons from ^{18}F-FDG. This problem can be partially solved by increasing NaI crystal thickness. On the other hand, the thicker crystal has the disadvantage of reducing spatial resolution for lower energy gamma ray detection. The gamma ray energy of radioisotopes used in conventional SPECT is around 140 keV, which is much lower than that of FDG (140 keV vs. 511 keV).

Although a choice of a coincidence gamma camera commonly involves increasing the thickness of the NaI crystal, a compromise between the 511 keV photon detection efficiency and the spatial resolution at low energy detection has to be made for one camera to conduct both single photon imaging and FDG imaging.[7] The clinical potential of a coincidence gamma camera for FDG imaging in oncologic diagnosis has been reported,[7–14] but few articles have demonstrated the clinical utility of one coincidence gamma camera with thick NaI crystals to conduct both single photon imaging and FDG imaging.

In this study the clinical feasibility of the dual-head coincidence gamma camera with thick (19 mm) NaI crystals was investigated by comparing the FDG images obtained with a dedicated PET camera, and ^{99m}Tc images obtained with a conventional gamma camera with thin (9.5 mm) NaI crystals.

MATERIALS AND METHODS

Imaging devices

A coincidence gamma camera (PCD®, Picker International, OH) has two rectangular (51 × 38 cm), large field of view detectors, with 19 mm (3/4 inch) NaI crystals. In the 2-dimensional acquisition mode, a slit collimator is attached to each of the detectors. The outward appearance of this camera is similar to a conventional dual-head gamma camera.

The dedicated PET camera with BGO crystals employed in this study is a SET 2400W (Shimadzu Corporation, Kyoto, Japan) with a 59.5 cm transaxial field of view and a 20 cm axial field of view which produces 63 image planes spaced 3.125 mm apart. The basic performance of the dual-head coincidence gamma camera and of the dedicated PET camera are summarized in Table 1.

The conventional gamma camera used for the evaluation of bone scan had two rectangular detectors (51 × 38 cm), and a large field of view, with 9.5 mm (3/8 inch) NaI crystals (Prism 2000®, Picker International, OH).

FDG imaging

A whole body image by means of the simultaneous emission-transmission method[15] with a rotating external source (370 MBq ^{68}Ge/^{68}Ga at installation) was initiated at 40 min after the injection of 185–370 MBq FDG by the multiple-bed position technique. The scanner hardware estimated and corrected for random events by means of the delayed-window technique. Scatter correction was not done. The software was set to provide up to seven bed increments (8-min acquisition per bed position). Four to five body sections including from head to thigh were imaged. Each data set was rebinned by single-slice rebinning and then reconstructed with an ordered subset expectation maximization (OS-EM) iterative algorithm (an ordered subset of 8 with a Butterworth prefilter with one iteration). The order and cut off frequency of the Butterworth prefilter were 8 and 0.32 cycle/pixel, respectively. Attenuation-corrected transaxial images with FDG were reconstructed into 128 × 128 matrices with pixel dimensions of 4.0 mm in-plane and 3.125 mm axially. The coronal images 9.8 mm slice thick were also produced from the transaxial images.

After completion of FDG imaging with the dedicated PET camera, patients underwent FDG imaging with the dual-head coincidence gamma camera at 100 min post-injection. A 15-ns timing window was employed to identify the coincidence events using the combination of photopeak-photopeak events, and Compton scatter-photopeak events. No Compton-Compton counts were accepted. The energy windows were set at 511 keV/30% for the ^{18}F photopeak and 280–340 keV for the Compton scatter events in the crystals. The random coincidence events were not corrected. All patients were imaged for 30 stops through a rotation of 180° per detector at 30 sec/frame for a total acquisition time of approximately 16 min per patient/bed position. The axial acceptance angle was set at 16°, and the transverse acceptance was set at 480 mm. The imaging area was determined from the CT or MRI findings. Image data were acquired in list mode and each item set was rebinned by single-slice rebinning. After the attenuation correction by Chang's method with

Table 1 The performance of the dual-head coincidence gamma camera and the dedicated PET camera

Performance	Dual-head coincidence[a] gamma camera	Dedicated[b] PET camera
Spatial resolution		
at 0 cm[c]	5.7 mm FWHM	4.5 mm FWHM
at 10 cm		
radial	6.2 mm FWHM	5.3 mm FWHM
tangential	5.8 mm FWHM	4.7 mm FWHM
Volume sensitivity	13 kcps/μCi/ml	270 kcps/μCi/ml
Scatter fraction	21%	13%

*reconstructed transaxial resolution

[a] PCD® (Picker, OH)

[b] SET 2000W (Shimadzu Corporation, Kyoto, Japan)

[c] at the center of field of view

an attenuation coefficient of 0.095 cm^{-1}, the projection data were used to generate the transaxial images with the OS-EM method (order subset of 8 with 3 iterations). Finally, the reconstructed transaxial images were processed with a Butterworth filter (order 8, cut off level 0.35 cycle/pixel). The images were generated into a 128 × 128 matrix with 9.8 mm slice thickness. The coronal images were also produced from the transaxial images. One section including the lesions was imaged in this study.

Whole body bone scan

The whole body bone images were obtained with a dual-head coincidence gamma camera equipped with a low-energy high resolution collimator 3 hours after the injection of 740 MBq ^{99m}Tc hydroxymethylene diphosphonate (HMDP). The scan speed was 9 cm/min and the images were generated in 512 × 1024 matrices. After the completion of imaging with the dual-head coincidence gamma camera, whole body imaging was sequentially conducted with a conventional dual-head gamma camera with thin (9.5 mm) NaI crystals. The scan speed, image matrix size, and the distance between detector and patient were the same as for the bone imaging with the dual-head coincidence gamma camera.

Patients population

Twenty-seven patients (20 men, 7 women: 33–80 y) with known or suspected malignant tumors were subjected to the comparative study of FDG images obtained with the dual-head coincidence gamma camera and the dedicated PET camera. They included 12 patients with lung cancer, 4 patients with esophageal cancer, 3 patients with soft tissue tumor (2 neurinoma and 1 liposarcoma), 3 patients with metastatic bone tumors of prostatic cancer, 2 patients with malignant lymphoma of the abdomen, 1 patient with primary bone tumor (chondroblastoma), 1 patient with paraaortic lymph node metastasis of uterine cancer, and 1 patient with head and neck cancer (acinic adenocarcinoma). Fifty-four tumor lesions in 27 patients were evaluated for FDG uptake. The neoplasms in twenty-eight lesions were histologically proven by biopsy or surgical pathology, including 25 malignant tumors and three benign tumors with 2 neurinomas and 1 chondroblastoma. The diagnoses of the other 26 lesions were based on the CT/MRI/US findings and clinical follow-up for 5 months.

Ten patients with suspected metastatic bone tumors (5 men, 5 women: 40–72 y) were enrolled in the comparative study of whole body bone imaging. There were 5 patients with breast cancer and 5 patients with prostatic cancer.

All patients gave written informed consent before a PET study and bone scan.

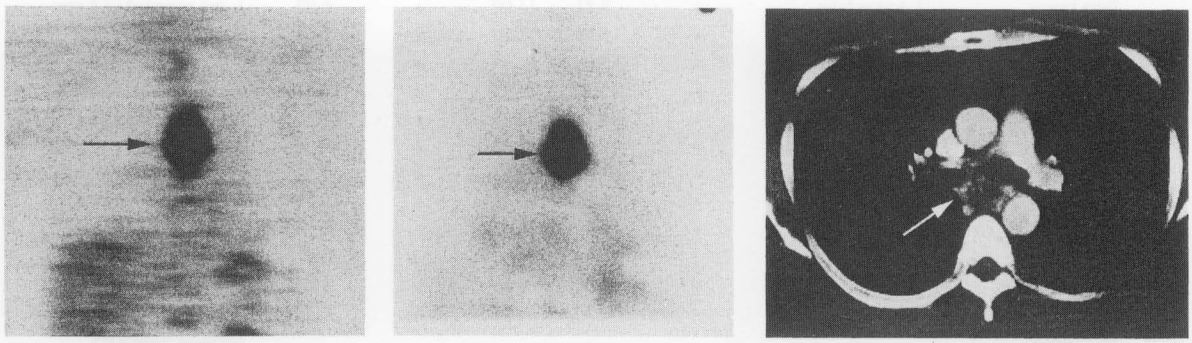

a b c

Fig. 1 A case of esophageal cancer. Both the coronal section of the FDG image obtained with the dedicated PET camera (a) and that obtained with the dual-head coincidence gamma camera (b) revealed the primary lesion (arrow) showing on the CT image (c).

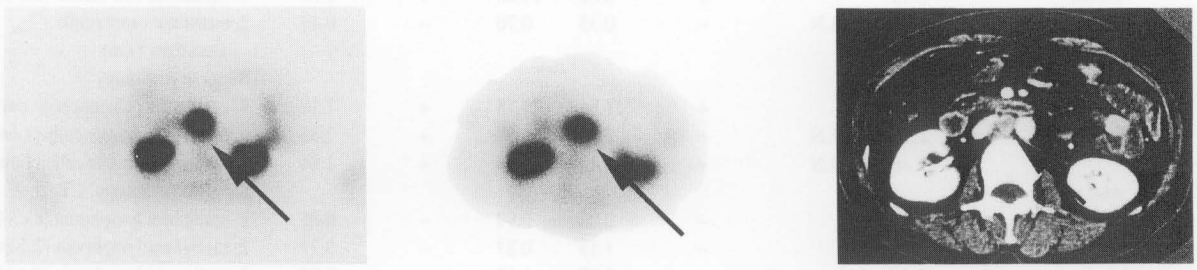

a b c

Fig. 2 Paraaortic lymph node metastasis in a patient with uterine cancer. Both transaxial FDG image obtained with the dedicated PET camera (a) and that obtained with the dual-head gamma camera (b) revealed a metastatic lymphadenopathy (arrow) showing on the CT image (c).

Table 2 Patients' characteristics and results of FDG imaging

Patient no.	Tumor	Sites	Regions	Dedicated PET camera			Coincidence gamma camera		Confirmation
				visual interpretation	SUV	T/B	visual interpretation	T/B	
1 72/M	lung cancer	1							Surgical pathology
			1. upper lobe	+	1.69	4.69	–	0.88	1. adenocarcinoma (2 cm)
2 72/M	lung cancer	4							Biopsy, CT, clinical follow-up
			1. upper lobe	+	3.82	15.92	+	3.20	1. small cell cancer (3 cm)
			2. mediastinal LN	+	4.49	18.71	+	5.10	2. not sampled (4 cm)
			3. rib	+	4.58	19.08	+	3.47	3. not sampled (4 cm)
			4. spine	+	2.32	9.67	+	3.46	4. not sampled (3 cm)
3 80/M	lung cancer	1							Biopsy, CT, clinical follow-up
			1. upper lobe	+	3.15	4.77	+	1.75	1. adenocarcinoma (3 cm)
4 66/M	lung cancer	1							Surgical pathology
			1. upper lobe	+	1.21	3.03	–	1.23	1. squamous cell cancer (1.8 cm)
5 66/M	lung cancer	1							Surgical pathology
			1. upper lobe	+	2.78	5.91	+	2.63	1. adenocarcinoma (2 cm)
6 78/M	lung cancer	2							Biopsy, CT, clinical follow-up
			1. lingula	+	8.27	18.80	+	3.59	1. squamous cell cancer (6 cm)
			2. mediastinal LN	+	1.91	4.34	+	2.33	2. not sampled (2.5 cm)
7 64/F	lung cancer	1							Surgical pathology
			1. lingula	–	0.82	1.34	–	0.98	1. Adenocarcinoma (2 cm)
8 70/M	lung cancer	1							Surgical pathology
			1. lower lobe	+	4.34	14.45	+	3.08	1. Squamous cell carcinoma (3 cm)
9 62/M	lung cancer	1							Biopsy, CT, clinical follow-up
			1. upper lobe	+	6.57	16.43	+	4.05	1. Squamous cell carcinoma (6 cm)
10 72/M	lung cancer	1							Biopsy, CT, clinical follow-up
			1. lower lobe	–	0.29	0.91	–	0.86	1. Squamous cell carcinoma (1 cm)
			2. mediastinal LN	+	4.47	13.97	+	3.18	2. not sampled (3 cm)
11 34/M	metastatic lung tumor (testicular cancer)	9							CT, clinical follow-up
			1. lower lobe	+	3.41	11.00	+	6.08	1. not sampled (2.5 cm)
			2. mediastinal LN	+	5.58	18.00	+	7.17	2. not sampled (3 cm)
			3. mediastinal LN	+	6.65	21.45	+	13.08	3. not sampled (3 cm)
			4. lower lobe	+	15.30	49.35	+	18.51	4. not sampled (4 cm)
			5. mediastinal LN	+	4.25	13.71	+	8.58	5. not sampled (2.5 cm)
			6. mediastinal LN	+	4.49	14.48	+	9.88	6. not sampled (3 cm)
			7. upper lobe	+	3.06	9.87	+	5.33	7. not sampled (2 cm)
			8. upper lobe	+	5.94	19.16	+	15.18	8. not sampled (3 cm)
			9. upper lobe	+	4.49	14.49	+	9.20	9. not sampled (3 cm)
12 33/F	metastatic lung tumor (breast cancer)	1							CT, clinical follow-up
			1. upper lobe	+	2.30	4.89	+	1.73	1. not sampled (8 cm)
			2. lower lobe	–	0.33	0.71	–	0.42	2. not sampled (1.7 cm)
13 56/M	esophageal cancer	1							Surgical pathology
			1. Im	+	1.82	3.08	+	2.35	1. squamous cell cancer (5.8 cm)
14 42/M	esophageal cancer	2							Biopsy, CT, clinical follow-up
			1. Im	+	3.67	5.56	+	4.73	1. squamous cell cancer (5 cm)
			2. regional LN	+	3.50	6.36	+	3.73	2. not sampled (3 cm)
15 50/M	esophageal cancer	1							Surgical pathology
			1. Ei	+	8.62	14.86	+	1.73	1. squamous cell cancer (5.6 cm)
			2. regional LN	–	0.33	0.70	–	0.41	2. metastatic cancer cells (less than 1 cm)
16 65/M	esophageal cancer	3							Surgical pathology
			1. Im	+	11.86	25.78	+	7.19	1. squamous cell cancer (7 cm)
			2. regional LN	+	2.80	6.09	+	2.05	2. metastatic cancer cells (1 cm)
			3. regional LN	+	2.45	5.33	+	1.84	3. metastatic cancer cells (1 cm)
17 37/F	malignant lymphoma	6							Surgical pathology, CT
			1. kidney	–	2.02	0.99	–	0.85	1. malignant lymphoma (8 cm)
			2. kidney	–	1.13	0.87	–	0.75	2. malignant lymphoma (2.5 cm)
			3. hilar LN	–	0.97	1.17	–	0.89	3. malignant lymphoma (2 cm)
			4. hilar LN	–	0.97	1.01	–	0.88	4. malignant lymphoma (2 cm)
			5. paraaortic LN	–	0.97	1.01	–	1.02	5. malignant lymphoma (1 cm)
			6. paraaortic LN	–	0.96	1.01	–	0.85	6. malignant lymphoma (1 cm)

Table 2 (continued)

18	73/F	malignant lymphoma	1 1. liver	 +	 4.53	 6.14	 +	 2.94	CT, clinical follow-up 1. not sampled (6 cm)
19	66/M	metastatic bone tumor (prostatic cancer)	3 1. spine 2. spine 3. spine	 – – –	 1.40 1.72 1.32	 1.06 1.30 1.01	 – – –	 1.21 1.01 0.72	CT, clinical follow-up 1. not sampled (n.d.) 2. not sampled (n.d.) 3. not sampled (n.d.)
20	73/M	metastatic bone tumor (prostatic cancer)	2 1. spine 2. spine	 – –	 1.19 1.25	 1.57 1.64	 – –	 0.78 0.77	CT, clinical follow-up 1. not sampled (n.d.) 2. not sampled (n.d.)
21	72/M	metastatic bone tumor (prostatic cancer)	2 1. spine 2. spine	 + +	 3.37 1.92	 3.62 2.06	 + +	 1.72 1.32	CT, clinical follow-up, bone scan 1. not sampled (n.d.) 2. not sampled (n.d.)
22	59/F	uterine cancer	1 1. paraaortic LN	 +	 3.14	 3.61	 +	 2.22	CT, clinical follow-up 1. not sampled (2.5 cm)
23	51/M	soft tissue tumor	1 1. thigh	 +	 1.91	 2.20	 +	 1.89	Surgical pathology, MRI 1. neurinoma (8 cm)
24	66/M	soft tissue tumor	1 1. knee	 +	 0.85	 1.55	 –	 1.15	Surgical pathology, MRI 1. liposarcoma (4 cm)
25	64/F	soft tissue tumor	1 1. leg	 +	 1.06	 1.96	 +	 2.23	Surgical pathology, MRI 1. neurinoma (3.5 cm)
26	33/M	soft tissue tumor	1 1. knee	 +	 1.83	 4.58	 +	 2.48	Surgical pathology, MRI 1. chondroblastoma (2 cm)
27	55/F	head and neck tumor	1 1. parotis	 +	 5.82	 5.54	 +	 3.45	Surgical pathology, CT 1. acinic adenocarcinoma (3.5 cm)

LN = lymph node, SUV = standardized uptake value, T/B = tumor to background count ratio, Im = middle portion of intrathoracic esophagus, Ei = inferior portion of intrathoracic esophagus

Table 3 Comparison of tumor detectability of the dual-head coincidence gamma camera and the dedicated PET camera

Sensitivity	Dual-head coincidence gamma camera	Dedicated PET camera	Results of McNemar's test
Patient basis (n = 27)	74.1% (20/27)	85.2% (23/27)	n.s.
Lesion basis (n = 54)	66.7% (36/54)	72.2% (39/54)	n.s.

Data analysis

All FDG images shown on the hard-copies were retrospectively interpreted by three experienced nuclear radiologists until a consensus was reached. At first the FDG images obtained with the dual-head coincidence gamma camera were reviewed, and then the FDG images obtained with the dedicated PET camera were interpreted in the limited area corresponding to the area of the FDG images obtained with the dual-head coincidence gamma camera. Compared with the surrounding background radioactivity, uptake scores of the lesions were called no uptake (–), faint uptake (+/–), moderate uptake (+), and definitely abnormal intense uptake (++). Moderate uptake (+) and definitely abnormal intense uptake (++) were called positive results for detecting tumors, and no uptake (–) and faint uptake (+/–) were called negative results. All FDG findings were finally compared to the standard conventional images such as CT, MR images, ultrasonography, and results of pathological diagnosis. Sensitivity of the dedicated PET camera and the dual-head gamma camera with FDG for detecting tumors was assessed on a patient basis and a lesion-by-lesion basis.

For the semiquantitative analysis of tumor accumulation of FDG, ROIs approximately 1-cm in diameter were manually placed on the FDG images over the area corresponding to the lesions, which included the site of maximal FDG accumulation. The ROIs for the background activity measurement were placed on the right lower lung field of the thoracic section, the lateral intra-abdominal cavity below the right kidney of the abdominal or pelvic section, and the right lateral cervical region of the cervical section, respectively. For semiquantitative analysis of the FDG images obtained with the dedicated PET camera, the functional images of the standardized uptake value (SUV) were derived from the reconstructed transaxial images obtained with the dedicated PET camera, body weight, injected dose of FDG, and the calibration factor. The ROI analysis for tumor uptake was conducted by a radiologist

with a knowledge of clinical and pathologic data. The location of the ROI of the lesion corresponded to CT and/or MRI findings. The average PET values or SUV per pixel of the ROI were called the FDG uptake values of the tumor or the background area. Tumor to background FDG uptake ratios on the FDG images obtained with the dual-head coincidence gamma camera were determined and compared with those obtained with the dedicated PET camera.

The whole body bone scintigram obtained with the dual-head coincidence gamma camera with thick (19 mm) NaI crystals was compared with that obtained with the conventional dual-head gamma camera with thin (9.5 mm) NaI crystals. For the semiquantitative analysis, ROIs, 9 pixels in size, were placed on the areas of abnormal tracer uptake, the 5th lumbar spine on the posterior view image, the sternum on the anterior view image, and the soft tissue region over the thigh on the posterior view image as a background area. The counts in the ROI were divided by total counts in the field of view and the ratio was expressed as % uptake. The linear correlation between the % uptake derived from the bone images obtained with the dual-head coincidence camera and those derived from the bone images obtained with the conventional dual-head gamma camera was assessed.

Statistical analysis

The differences in the sensitivity of detecting tumors were statistically analyzed with McNeamar's test. The mean difference in the semiquantitative data was statistically evaluated by Student t-test. The linear correlations were assessed by a linear regression analysis. In all statistical analyses of this study, p value less than 0.05 was defined as significant.

RESULTS

Both FDG images obtained with the dual-head coincidence gamma camera and those obtained with the dedicated PET camera revealed 36 lesions in 20 patients (Figs. 1, 2). Three lesions in 3 patients showed positive results on the FDG images obtained with the dedicated PET camera and negative results on those derived from the dual-head coincidence gamma camera. Neither FDG image could not detect fifteen lesions in 7 patients (Table 2). The compared sensitivity of the dual-head coincidence gamma camera to the dedicated PET camera was 87.0% on a patient basis, and 92.3% on a lesion basis.

In either patient-basis sensitivity or lesion-basis sensitivity, there were no significant differences between the FDG images obtained with the dual-head coincidence gamma camera and those with the dedicated PET camera (Table 3). The tumor to background FDG uptake ratios of 54 lesions derived from the FDG images obtained with the dual-head coincidence gamma camera were significantly lower than those derived from the FDG images obtained with the dedicated PET camera (mean ± s.d.; 3.48 ± 3.77 vs. 8.12 ± 8.92, $p < 0.0001$, $n = 54$), but there was a significant linear correlation between the two ($y = 0.344x + 0.596$, $r = 0.84$, $n = 54$, $p < 0.001$) (Fig. 3).

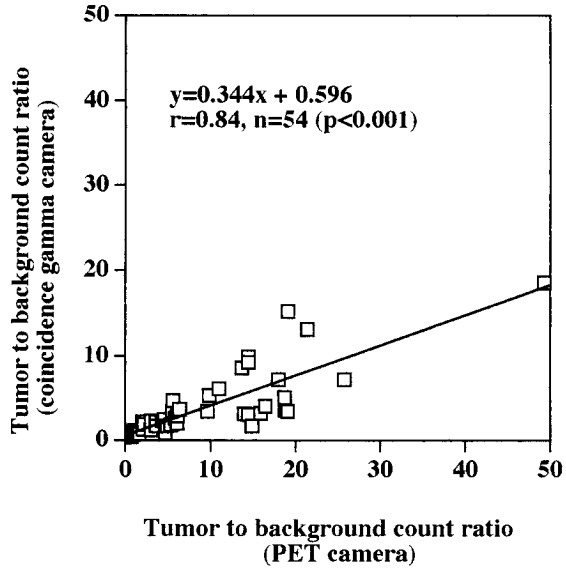

Fig. 3 Relationship of tumor to background FDG uptake ratios derived from the FDG images obtained with the dual-head coincidence gamma camera and those derived from the images by a dedicated PET camera. There was a significant linear correlation between the two.

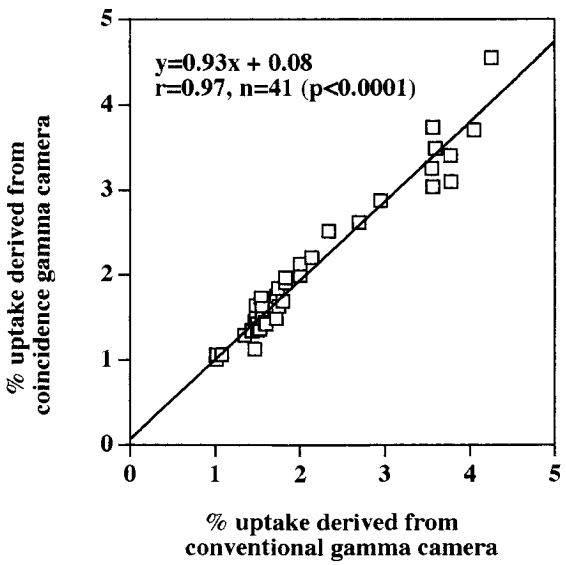

Fig. 4 Relationship of bone uptake (% uptake) derived from the dual-head gamma camera with thick NaI crystals and that derived from the conventional dual-head gamma camera with thin NaI crystals. A significant linear correlation was observed.

There were three abnormal bone scans and 7 normal bone scans with ^{99m}Tc-HMDP. Bone images of ^{99m}Tc reagents obtained with the dual-head coincidence gamma

camera with thick (19 mm) NaI crystals were quite similar to the images obtained with the conventional dual-head gamma camera with thin (9.5 mm) NaI crystals. The % uptake of ^{99m}Tc-HMDP was assessed in 41 sites including 11 suspected metastatic lesions. There was no significant difference between the % uptake derived from the bone images obtained with the dual-head coincidence gamma camera with thick (19 mm) NaI crystals and that from the bone images obtained with the conventional dual-head gamma camera with thin (9.5 mm) NaI crystals (mean ± s.d.; 2.01 ± 0.89 vs. 2.07 ± 0.93, n = 41, n.s.). There was a strong linear correlation between the two ($y = 0.93x + 0.08$, $r = 0.97$, $n = 41$, $p < 0.0001$) (Fig. 4).

DISCUSSION

Although the performance of the dual-head coincidence gamma camera was inferior to that of the dedicated PET camera (Table 1), its sensitivity in detecting tumors was not significantly different from that of the dedicated PET camera (Table 3). Neither the dual-head coincidence camera nor the dedicated PET camera could detect fifteen lesions, viz. 3 lung tumors, 5 regional lymph node metastatic lesions, 2 renal lesions, 5 metastatic skeletal lesions of spines of prostatic cancer. Most of them were lesions less than 1 cm in diameter with less than 1.0 SUV, or lesions located near the physiological FDG uptake such as the genitourinary tract. Although 2 lung cancer lesions and 1 liposarcoma of the knee were detected by the dedicated PET camera, they were not detected by the dual-head coincidence gamma camera. The two lung cancer lesions were 1.8 cm in diameter with 1.69 SUV, and 2 cm in diameter with 1.21 SUV. Although the liposarcoma was 4 cm in diameter (Table 2), the contrast-enhanced area on MR images was limited to less than 2 cm. The results of lesion-basis sensitivity revealed that the feasibility of FDG imaging with the dual-head coincidence gamma camera for detecting tumors less than 2 cm in diameter with less than 1.5 SUV was problematic. It may be due to the relatively low volume sensitivity and the limited spatial resolution in positron coincidence detection with a NaI crystal (Table 1) or insufficient attenuation correction by the calculation method. Although the lesion to background ratio obtained with the dual-head coincidence gamma camera correlated well with that obtained with the dedicated PET camera (Fig. 3), it was significantly lower. Utilization of measured attenuation correction with the external radionuclide may solve this problem.[4,11,12] Sensitivity in detecting the malignant tumor with the dual-head gamma camera relative to that with the dedicated PET camera was 92.3% in this study. The relative sensitivities previously reported varied widely from 53% to 100%.[8,9,11–14] The relative sensitivity was influenced by the patient population, lesion size and its location, the FDG tumor uptake, and the efficiency of the dedicated PET camera employed in the clinical study. FDG imaging with the coincidence gamma camera has a high sensitivity of more than 95% in detecting pulmonary lesions.[9–11] A recent study of FDG PET revealed that the tumor to background ratio increased with time after the injection, and delayed imaging was recommended for tumor detection.[16] Since the imaging with the dual-head gamma camera was started after the completion of imaging with the dedicated PET camera in this study, the dual-head gamma camera was in an advantageous position vis-a-vis the dedicated PET camera.

An important advantage of the coincidence gamma camera is the feasibility of conventional single photon imaging such as whole body scan and SPECT in addition to FDG positron imaging. Since a thin 9.5 mm thick NaI crystal, usually employed in the conventional gamma camera, has low efficiency for stopping 511 keV photons inside the crystal, thicker NaI crystals ranging from 15.9 mm (5/8 inch) to 25.4 mm (1 inch) are likely to be employed in the dual-head coincidence gamma camera. The disadvantage of the thick crystals is the resultant reduction in the spatial resolution for detecting low-energy gamma rays. A compromise between the 511 keV detection and the spatial resolution at low-energy detection has to be made for one camera, but the whole body images with ^{99m}Tc-HMDP obtained with the dual-head gamma camera were quite similar visually and quantitatively to those obtained with the conventional gamma camera with thin (9.5 mm) crystals (Fig. 4). Single photon imaging with the dual-head coincidence camera with thick crystals was clinically acceptable for nuclear medicine diagnosis.

CONCLUSION

The dual-head coincidence gamma camera with thick NaI crystals has potentially high clinical applicability for community hospitals.

REFERENCES

1. Coleman RE. Clinical PET in oncology. *Clin Pos Imag* 1998; 1: 15–29.
2. Kim EE, Chung SK, Haynie TP, Kim CG, Cho BJ, Podoloff DA, et al. Differentiation of residual or recurrent tumors from post-treatment changes with F-18 FDG PET. *Radiographics* 1992; 12: 269–279.
3. Inoue T, Kim EE, Komaki R, Wong FC, Bassa P, Wong WH, et al. Detecting recurrent or residual lung cancer with FDG-PET. *J Nucl Med* 1995; 36: 788–793.
4. Martin WH, Delbeke D, Patton JA, Sandler MP. Detection of malignancies with SPECT versus PET, with 2-[Fluorine-18]fluoro-2-deoxy-D-glucose. *Radiology* 1996; 198: 225–231.
5. Macfarlane DJ, Cotton L, Ackermann RJ, Minn H, Ficaro EP, Schreve PD, et al. Triple-head SPECT with 2-[fluorine-18]fluoro-2-deoxy-D-glucose (FDG): initial evaluation in oncology and comparison with FDG PET. *Radiology* 1995;

194: 425–429.
6. Muehllehner G, Geagan M, Countryman P, Nellemann P. SPECT scanner with PET coincidence capability. [abstract] *J Nucl Med* 1995; 36: 70P.
7. Abdel-Dayem HM, Luo JQ. Clinical experience with dual head gamma camera coincidence imaging. *Clin Pos Imag* 1999; 2: 31–39.
8. Shreve PD, Steventon RS, Deteres EC, Kison PV, Gross MD, Wahl RL. Oncologic diagnosis with 2-[fluorine-18]fluoro-2-deoxy-D-glucose imaging: Dual-head coincidence gamma camera versus positron emission tomographic scanner. *Radiology* 1998; 207: 431–437.
9. Weber WA, Neverve J, Sklarek J, Ziegler SI, Bartenstein P, King B, et al. Imaging of lung cancer with fluorine-18 fluorodeoxyglucose; comparison of a dual-head gamma camera in coincidence mode with a full-ring positron emission tomography system. *Eur J Nucl Med* 1999; 26: 388–395.
10. Weber W, Young C, Abdel-Dayem HM, Sfakianakis G, Weir GJ, Swaney CM, et al. Assessment of pulmonary lesions with ^{18}F-fluorodeoxyglucose positron imaging using coincidence mode gamma cameras. *J Nucl Med* 1999; 40: 574–578.
11. Tatsumi M, Yutani K, Watanabe Y, Miyoshi S, Tomiyama N, Johkoh T, et al. Feasibility of fluorodeoxyglucose dual-head gamma camera coincidence imaging in the evaluation of lung cancer: comparison with FDG PET. *J Nucl Med* 1999; 40: 566–573.
12. Zimny M, Kaiser HJ, Cremerius U, Reinartz P, Schreckenberger M, Sabri O, et al. Dual-head gamma camera 2-[fluorine-18]-fluoro-2-deoxy-D-glucose positron emission tomography in oncological patients: effects of non-uniform attenuation correction on lesion detection. *Eur J Nucl Med* 1999; 26: 818–823.
13. Delbeke D, Patton JA, Martin WH, Sandler MP. FDG PET and dual-head gamma camera positron coincidence detection imaging of suspected malignancies and brain disorders. *J Nucl Med* 1999; 40: 110–117.
14. Boren EL, Delbeke Jr D. Patton JA, Sandler MP. Comparison of FDG PET and positron coincidence detection imaging using a dual-head gamma camera with 5/8-inch NaI(Tl) crystals in patients with suspected body malignancies. *Eur J Nucl Med* 1999; 26: 379–387.
15. Inoue T, Oriuchi N, Kunio M, Tomiyoshi K, Tomaru Y, Aoyagi K, et al. Accuracy of standardized uptake value measured by simultaneous emission and transmission scanning in PET oncology. *Nucl Med Commun* 1999; 20: 849–857.
16. Kubota K, Yamaguchi K, Ito M, Ohira H, Yamada K, Fukuda H. Whole body FDG-PET for tumor detection should be imaged at 2 hr after injection. *J Nucl Med* 1999; 40: 141P.